



**HAL**  
open science

# On the applicability of Persistent Scatterers interferometry (PSI) analysis for long term CO<sub>2</sub> storage monitoring

Jeremy Rohmer, Daniel Raucoules

► **To cite this version:**

Jeremy Rohmer, Daniel Raucoules. On the applicability of Persistent Scatterers interferometry (PSI) analysis for long term CO<sub>2</sub> storage monitoring. *Engineering Geology*, 2012, 147-148, pp.137-148. 10.1016/j.enggeo.2012.07.010 . hal-00733360

**HAL Id: hal-00733360**

**<https://brgm.hal.science/hal-00733360>**

Submitted on 18 Sep 2012

**HAL** is a multi-disciplinary open access archive for the deposit and dissemination of scientific research documents, whether they are published or not. The documents may come from teaching and research institutions in France or abroad, or from public or private research centers.

L'archive ouverte pluridisciplinaire **HAL**, est destinée au dépôt et à la diffusion de documents scientifiques de niveau recherche, publiés ou non, émanant des établissements d'enseignement et de recherche français ou étrangers, des laboratoires publics ou privés.

1                   **On the applicability of Persistent Scatterers**  
2                   **interferometry (PSI) analysis for long term CO<sub>2</sub>**  
3                   **storage monitoring**

4                   Jeremy Rohmer<sup>\*1</sup>, Daniel Raucoules<sup>\*</sup>

5                   *\*BRGM, Natural Risks Division, 3, av. Claude Guillemin BP 36009, 45 060 Orléans Cedex 2, FRANCE*

7                   **Abstract**

8                   Persistent scatterers synthetic aperture radar interferometry (PSI) analysis is viewed as a  
9                   promising monitoring technique for multiyear detection of ground surface displacements  
10                  during long term CO<sub>2</sub> injection into deep aquifers (of the order of 25 to 50 years).  
11                  This technique was successfully utilized at the CO<sub>2</sub> storage site of In-Salah (Algeria).  
12                  Nevertheless, this success may not be generalized to future onshore industrial-scale CO<sub>2</sub>  
13                  storage sites, which are planned in far more complex contexts mostly presenting natural  
14                  terrains, either agricultural or vegetated areas, i.e. characterized by poor PS density, which  
15                  might locally drop to zero, hence hampering the deployment of the PSI technique. The  
16                  objective of the present paper is to discuss the constraints on the PSI application regarding the  
17                  specificities (magnitude, spatial or temporal scales and evolution) of the deformation  
18                  phenomenon associated with the CO<sub>2</sub> injection into storage aquifers. This discussion is  
19                  supported by the estimates of the expected spatio-temporal evolution of surface vertical  
20                  displacements caused by CO<sub>2</sub> injection in deep aquifers by combining the approximate  
21                  solutions for pressure build-up and for the associated vertical displacements in an elastic half-

---

<sup>1</sup> Corresponding author. Tel.: + 33-2-38-64-30-92; fax: + 33-2-38-64-30-92.  
E-mail address: [j.rohmer@brgm.fr](mailto:j.rohmer@brgm.fr) (J. Rohmer).

22 space. A possible option to enhance the performance of the PSI technique is explored, namely  
23 the deployment of a network of corner reflectors CR corresponding to artificial devices  
24 installed on ground to complement the existing “natural” PS network. A methodology is then  
25 proposed to optimize the CR network (number and position) in an iterative strategy (e.g.,  
26 every 10 years) relying on the prediction of surface deformation. The methodology is  
27 illustrated by a CO<sub>2</sub> injection scenario in the Paris basin context.

28

29 Keywords: CO<sub>2</sub> geological storage; Monitoring protocol; InSAR remote sensing; Persistent  
30 Scatterers; geomechanical model; Corner Reflectors.

31

## 32 **Introduction**

33 CO<sub>2</sub> capture and geological storage (denoted CCS) is seen as a promising technology in the  
34 portfolio of measures required to mitigate the effects of anthropogenic greenhouse gas  
35 emissions (IPCC, 2005). Among the available geological targets, deep aquifers are recognized  
36 to offer very large potential storage capacity with a broad distribution throughout the world in  
37 all sedimentary basins (e.g., IPCC, 2005). Therefore, the present paper will primarily focus on  
38 this option. The International Energy Agency (IEA) recently evaluated the contribution of  
39 CCS to emissions reductions by 2050 to one fifth in order to achieve the most cost-effective  
40 stabilisation of greenhouse gas concentrations (IEA, 2009). On this basis, the IEA concludes  
41 that the implementation of the technology should reach 100 projects in 2020, and more than  
42 3000 in 2050 representing an amount of 10 Gt of CO<sub>2</sub> stored per year. These figures highlight  
43 the large number of storage sites that shall be operated. Nevertheless, a prerequisite to any  
44 CCS large scale industrial development is the demonstration that the storage is both efficient  
45 and safe as outlined by the European directive on geological storage of carbon dioxide

46 (directive 2009/31/EC, April 2009). In this context, monitoring techniques constitute a key  
47 component of any CO<sub>2</sub> storage risk management strategy aiming at providing information on  
48 the CO<sub>2</sub> fate (migration and trapping) within the reservoir and demonstrating that CO<sub>2</sub>  
49 containment is effective (e.g., Benson, 2006).

50 Among the possible monitoring techniques, the space-borne Differential SAR (Synthetic  
51 Aperture Radar) interferometry may constitute a promising and cost-effective option, as it can  
52 provide valuable information on surface deformation induced by volumetric changes through  
53 time and space resulting from CO<sub>2</sub> injection in deep aquifers (Tamburini et al., 2010). This  
54 technique uses the phase of the radar signal in order to derive an estimation of the  
55 displacement of the ground surface between two passes of the satellite over the area. Further  
56 details can be found for instance in Raucoules et al. (2007). The basic idea is that (once  
57 removed flat earth and topographic components) the phase difference is proportional (modulo  
58  $2\pi$ ) to the Line of Sight displacement occurred between the two acquisitions (assuming that  
59 we can identify a stable reference area on the image. If not, the displacement is obtained with  
60 an unknown constant value offset). A major interest of the technique lies on the fact that the  
61 spatial sensor is able to image the ground surface regularly (presently, repetitiveness varies  
62 depending on characteristics of the available satellites between few days to more than one  
63 month).

64 Yet, one major limitation results from the temporal decorrelation phenomena (Zebker and  
65 Villasenor, 1992) stemming from changes in the physical (e.g. dielectric characteristics) or  
66 geometric (e.g. the distribution inside of the image elementary cell) characteristics of the  
67 backscattering objects. Multi-temporal processing of interferometric series is generally  
68 needed to cope with this shortcoming. Among the possible multi-temporal techniques, PSI  
69 (Persistent Scatterers Interferometry – e.g. Ferreti et al., 2000) are advanced techniques based  
70 on the processing of numerous, typically more than 30, images to identify a network of

71 persistent, temporally stable, highly reflective ground features -persistent scatterers (denoted  
72 PS). These scatterers typically are cultural features of the developed landscape such as  
73 buildings, utility poles, roadways, etc., but also natural stable elements with stable and strong  
74 backscattering characteristics (such as stable rocks with specific orientation).

75 To date, such space-borne techniques have been successfully used in a variety of domains  
76 involving subsurface fluid withdrawal / injection and surface deformation response, for  
77 instance groundwater flow characterization in complex aquifers systems (Bell et al., 2008), oil  
78 / gas fields characterization (e.g., Vasco et al., 2008a), monitoring of seasonal gas storage  
79 (e.g., Teatini et al., 2011). More recently, surface deformation have been measured at In Salah  
80 Gas Project in Algeria, where 0.5–1 million tonnes CO<sub>2</sub> per year have been injected over the  
81 past 5 years (e.g. see site context described by Rutqvist et al., 2010). This analysis revealed an  
82 average ground uplift of 5 mm/year and allowed getting better insight not only in the CO<sub>2</sub>  
83 migration at depth (e.g., Mathieson et al., 2009), but also in the behaviour of the storage  
84 reservoir (e.g., Vasco et al., 2008b) and of the storage complex during injection operations  
85 (e.g., Rutqvist et al., 2010).

86 However, such a successful result might not be easily generalised to any onshore CO<sub>2</sub> storage  
87 sites, because the In Salah case is characterized by very favourable conditions for the  
88 implementation of the PSI technique, the site being located in an arid region so that the  
89 Permanent Scatterer PS density is very high, exceeding 1,000 per km<sup>2</sup> (300,000 PS used by  
90 Tamburini et al., 2010 over an area of approximately 10 km by 15 km).

91 The objective of the present paper is to get a better insight in the applicability of the Persistent  
92 Scatterers Interferometry implementation regarding the conditions of the future storage sites  
93 and the specificities of the expected ground deformation phenomenon, i.e. the expected  
94 spatio-temporal evolution of surface displacements caused by CO<sub>2</sub> injection operations at  
95 depth.

96 The remainder of the paper is organized as follows. We estimate in a first section the expected  
97 surface displacements by means of an analytical model. Though inherently based on  
98 simplifications, the analytical results allow investigating a large variety of injection scenarios  
99 (e.g. depth, injection rate, storage aquifer characteristics, etc.) useful to support the discussion  
100 in section 2. Given the discussed limitations for the CO<sub>2</sub> storage context, we propose to  
101 explore, in a third section, a possible strategy to enhance the performance of the PSI technique  
102 for CO<sub>2</sub> storage monitoring by deploying a network of “artificial” PS, i.e. corner reflectors CR  
103 (e.g., Novali et al., 2005) in an iterative design approach over the whole injection duration.  
104

## 105 **1. Estimates of the expected spatio-temporal evolution ground**

### 106 **vertical displacements**

107 In this section, we briefly describe an analytical solution for assessing ground displacement  
108 assessment during CO<sub>2</sub> injection in deep aquifers (section 1.1). Details of the analytical model  
109 are provided in Appendix A and B. This model is then applied to a typical injection scenario  
110 (section 1.2) and its applicability is discussed (section 1.3).

#### 111 ***1.1. Analytical solution for ground displacement assessment***

112 In the present article, the expected spatio-temporal evolution of ground vertical displacements  
113 due to CO<sub>2</sub> injection at depth are estimated using an analytical model developed by  
114 combining :

- 115 - the approximate solutions for pressure build-up (i.e. the pressure increase due to  
116 injection) during CO<sub>2</sub> injection in brine aquifers of very large spatial extent (seen as  
117 open systems) based on the studies of Mathias et al. (2009a&b);

118 - the poro-elastic solution for vertical surface displacements estimate in an elastic half-  
119 space, originally developed in the field of hydrocarbon and geothermal activities by  
120 considering an axi-symmetric thin disk reservoir with general reservoir pressure  
121 distribution (Segall, 1992; Segall and Fitzgerald, 1998).

122 For sake of clarity, the main assumptions and formulations of both analytical solutions are  
123 respectively described in Appendix A and B. Noteworthy, each of these solutions have been  
124 validated through numerical simulations (Mathias et al., 2009a) or against in situ observations  
125 (at Lacq in southern France, see Segall, 1992).

## 126 ***1.2. Analysis of a typical injection scenario***

127 We assess the spatio-temporal evolution of ground vertical displacements resulting from a  
128 typical scenario corresponding to 1 Mt/y CO<sub>2</sub> injection during 25 years into a saline aquifer  
129 formation at 1500m depth. Considering a pressure and geothermal gradient of respectively  
130  $\approx 10^5$  Pa/m and 0.03 °C/m, the initial pressure and temperature are of 15 MPa and 45 °C at  
131 1500m depth. The homogeneous properties of the aquifer formation are typical of  
132 sedimentary formations suitable for CO<sub>2</sub> storage, with high-enough permeability and porosity  
133 (see for instance Birkholzer et al., 2009 for typical hydrogeological properties and Rohmer  
134 and Seyed, 2010 for typical geomechanical properties) and are summarized in Table 1.

135

136 *[Table 1 about here]*

137

138 Figure 1 depicts the spatial distribution of changes in vertical ground displacements estimated  
139 using the equations described in Appendix A and B. Different injection durations are  
140 considered and vary from 1 month to 25 years. The pressure build-up reaches a maximum  
141 value within the injector near-zone and decreases deeply in an exponential fashion within the  
142 CO<sub>2</sub> plume region (the extent being marked by the steep decrease of the pressure build-up in

143 Figure 1A) and linearly within the brine-filled region. The vertical surface displacements  
144 follow the same trend (Figure 1B), but with a smoother form of the spatial distribution so that  
145 these are approximately constant over approximately 1 km and steeply decrease reaching (and  
146 even exceeding) the lateral extent of the pressurized zone at depth (i.e. the zone for which the  
147 pressure build-up is non-nil). For instance, after 2 years of injection, the vertical surface  
148 displacements exceed 4 mm over the lateral distance range of 0 to 1 km and decrease reaching  
149 ~10 km given that the extent of the pressurized zone reaches ~8 km. The smooth spatial  
150 distribution is explained by cumulative contribution of all the rings of dilation with magnitude  
151 proportional to the pressure build-up (i.e. decreasing with the lateral distance) as shown in  
152 Appendix (Figure 9).

153 Let us consider the gradient (in absolute value) of displacements corresponding to the  
154 difference between vertical displacements respectively observed at positions  $\vec{r}$  and of  $\vec{r} + \vec{\Delta}$   
155 divided by the distance  $\|\vec{\Delta}\|$ , where  $\|\vec{\Delta}\|$  is the characteristic length of a satellite image pixel  
156 (typically between 10 and 50 m depending on sensor and processing). This gradient is largely  
157 smaller than the maximum allowed value corresponding to half a fringe per pixel, *i.e.* of about  
158  $1.5 \text{ cm}/10\text{m}=1.5 \times 10^{-3}$  to  $1.5\text{cm}/50\text{m}=3 \cdot 10^{-4}$  for vertical movements with ERS data (Raucoules  
159 et al., 2007). This value would be modified for sensors with different resolutions and  
160 wavelengths, the maximum measurable gradient being proportional to wavelength and  
161 inversely proportional to pixel size. Even in case of a point-based method (such as PSI  
162 techniques) with larger  $\|\vec{\Delta}\|$ , typically ranging 500m to 1000m in rural zones (in this case  $\|\vec{\Delta}\|$   
163 does not correspond to the pixel size, but to the distance between PS), this maximum  
164 measurable gradient should not be theoretically a limitation, because the expected total  
165 deformation of the order of ~1 cm, as shown in Figure 1B, corresponds to less than one C-  
166 band sensor fringe (equivalent to ~3 cm of vertical displacement).

167 *[Figure 1 about here]*

168 Considering the temporal evolution of the maximal surface displacement within the injector  
169 near-zone, Figure 2 shows that it reaches a maximum value of ~11 mm over a time span of 25  
170 years and evolves following a logarithmical function over time. This trend is partly explained  
171 by the temporal evolution of the maximum pressure build-up within the injector near-zone.  
172 But, given its rapid evolution (after 1 month of injection, it reaches more than 85 % of the  
173 maximal pressure build-up), the temporal evolution is in great part explained by the  
174 cumulative contributions of rings of dilation, as shown in Figure 9, (Appendix A), whose  
175 number increases over time as the pressure front propagates within the aquifer formation.

176 *[Figure 2 about here]*

### 177 ***1.3. Applicability of the analytical solution***

178 The described analytical model is proposed as a quick-assessment tool, which should be used  
179 to capture the general trend of surface deformation due to CO<sub>2</sub> injection, i.e. to estimate  
180 orders of magnitude of the expected vertical displacements either to assess the likelihood of a  
181 risk event associated with ground surface perturbations in a preliminary risk analysis of the  
182 storage site (e.g., Bouc et al., 2011), or, as proposed in the present paper (section 2 & 3), to  
183 investigate the applicability of the PSI analysis considering a broad range of different  
184 scenarios. Noteworthy, the application of the model to the In-Salah's case considering rock  
185 properties and injection scenario described by Vasco et al. (2010) produces a measurable  
186 surface displacement of approximately 4 mm/y, i.e. in the order of what has been actually  
187 measured.

188 An in-depth understanding of the surface deformation process due to CO<sub>2</sub> injection at depth  
189 should consider several aspects, which the analytical model hardly accounts for, most of them  
190 being related to the complexity of both the deformation processes and the geological  
191 subsurface structure.

192 The described model assumes poro-elastic rock behaviour, hence implying that uplift  
193 instantaneously follows linearly the reservoir volumetric increase. Though confirmed through  
194 in situ compaction measurements (see e.g. the Groningen field, studied by Mobach and  
195 Gussinklo, 1994), a nonlinear dependence may also appear in some cases. See detailed  
196 discussion by Hettema et al. (2002). Furthermore, the ground deformation processes may be  
197 complicated by the presence of soils and unconsolidated rocks near the surface (e.g., Singh,  
198 1992).

199 The proposed model considers an idealized view of the subsurface structure so that both the  
200 reservoir and the surrounding rock are considered homogeneous and having the same material  
201 properties. Yet, aquifer formations targeted for CO<sub>2</sub> storage are mostly located within large  
202 sedimentary basins, which can be viewed as multi-layered systems (see e.g., Birkholzer et al.,  
203 2009). Analytical models have been proposed to account for this aspect (Fokker and Orlic,  
204 2006) and can be extended as a future direction of research to the CO<sub>2</sub> storage case in the  
205 similar approach as proposed in section 1. Furthermore, the presence of geologic  
206 discontinuities (i.e. the existence of faults) may increase ground movement potential, but on a  
207 localized spatial scale, as numerically demonstrated by Rutqvist et al., (2010).

## 208 **2. Constraints on the implementation of PSI technique**

209 In turn, we examine constraints to the implementation of the PSI technique regarding the  
210 specificities of the deformation phenomenon associated with the CO<sub>2</sub> injection at depth, in  
211 terms of magnitude (section 2.1), spatial and temporal scales (section 2.2 and 2.3) and  
212 evolution (section 2.4). Table 2 summarizes the constraints on the PSI implementation and the  
213 needs in terms of sensor characteristics in order to address the issues resulting from the  
214 expected motion characteristics.

215 *[Table 2 about here]*

## 216 ***2.1. Magnitude of the deformation***

217 It is difficult to determine beforehand whether the specific deformation phenomenon  
218 associated with the CO<sub>2</sub> injection at depth (as illustrated by the typical injection scenario  
219 described in section 1.3), may be monitored, because the feasibility and accuracy of PSI  
220 strongly depend on the number of satellite acquisitions and the temporal baselines (e.g.  
221 Hanssen, 2005).

222 The value of the precision PSI techniques has been widely discussed in the literature and can  
223 vary from less than 1 mm to centimeters. Colesanti et al. (2003) suggested that in an  
224 operational context under very good conditions (large data sets – i.e. >30 images, dense PS  
225 network, quasi linear deformation regimes), the precision could reach 0.5 mm/y for the annual  
226 deformation rate and 3 mm for the displacement values at given acquisition dates for PSI  
227 based on data from ERS, Envisat/ASAR or equivalent (C-band, resolution ~10m,  
228 repetitiveness of ~ 1 month). However, in less favourable cases (deformation rates higher than  
229 some cm/y, sparse PS, non-linear deformation) results could be worse. Studies based on inter-  
230 comparison of different PSI techniques and validation respect to ground measurements (see  
231 for instance Raucoules et al. 2009) showed that in unfavorable cases, the precision value can  
232 drop to 1.5 mm/y and the accuracy can be much worse (>5 mm/y). Furthermore, deformation  
233 superior to ~cm/y tends to be under-estimated if no prior assumption on the deformation is  
234 used in the processing (Raucoules et al., 2009). This issue is not expected for CO<sub>2</sub> storage  
235 applications as shown by the estimates of ground displacements resulting from a typical CO<sub>2</sub>  
236 injection scenario (see Figure 1B).

237 On this basis, a detection threshold for an individual deformation value of 5 mm (i.e. below  
238 which the deformation phenomenon is very unlikely to be detected) is considered in the  
239 present study. For the considered injection case in section 1.3, we show that deformation  
240 phenomenon associated with the CO<sub>2</sub> injection is likely to be detected only after the first year



266 and temporal decorrelation and allow (using statistical criteria) to compensate the atmospheric  
267 phase screens in order to improve the precision of the measurement. In urban area, buildings  
268 and other man-made structures often act as PS due to their corner reflector-like scattering  
269 behavior and high radar reflectivity so that we can obtain a very high density (hundreds per  
270 km<sup>2</sup>) of PS, even exceeding thousands per km<sup>2</sup> in arid regions (e.g., Bell et al., 2008).

271 However, the total area at ground surface to be affected by the deformation phenomenon  
272 caused by CO<sub>2</sub> injection at depth is expected to be very large in relation with the large over-  
273 pressurized zone at depth. Several authors have recently shown that the latter can reach of the  
274 order of several to more than a few tens of kilometers (e.g. Birkholzer et al., 2009). The  
275 detectable zone of deformation at surface will then be characterized by a lateral extent of the  
276 order of a few kilometers in the early stage of injection (ranging between 0.5 and less than 5  
277 km after 1 year of injection, Figure 3B, top) and of more than ten of kilometers (ranging  
278 between ~5 km and less than 15 km after 10 years of injection, Figure 3B, bottom). Such a  
279 large size of the monitored area implies that the size of the area covered by the satellite  
280 acquisitions (i.e. swath) should ideally be larger than 50 km. Yet, the larger the swath, the  
281 lower the resolution of the sensor. For instance, TerraSAR-X (mode scanSAR) presents a  
282 very large swath of 100km, but with a resolution of ~16m, which may be insufficient (see  
283 discussion below in section 2.3 and 2.4). Conversely, very high resolution sensors (~1m, such  
284 as TerraSAR-X or Cosmo-Skymed) offer insufficient coverage (~10km) and their use implies  
285 acquiring and processing a much larger amount of image data, which may become cost and  
286 resource intensive.

287 Furthermore, over such large areas, we can reasonably expect a vegetated cover (fields,  
288 forests, etc.) on a significant part of the storage site. For illustration purpose, the PICOREF  
289 sector in the Paris basin (of 3,455 km<sup>2</sup>, see location in Figure 6), where the potential  
290 implementation of CO<sub>2</sub> storage sites have been investigated (e.g. Grataloup et al., 2008), is

291 characterized by a land use composed of less than 5 % of artificial / urban areas and more  
292 than 95 % of natural (mainly forests) and agricultural areas. In such natural terrains, the  
293 absence of bright man-made structures might lead to sparse PS network (with density ~10 PS  
294 every km<sup>2</sup> to less than 1/km<sup>2</sup>). This constitutes a major obstacle to the phase unwrapping  
295 stage, where the solutions are directly dependent on the PS density and makes reliable  
296 estimation of deformation using PS techniques a challenging task.

297 The use of L-band data may contribute to improve the processing given that the vegetation is  
298 better penetrated using signal with short wavelength (e.g. Raucoules et al., 2007).  
299 Unfortunately there is currently, to the authors' knowledge, (and probably for the next 2  
300 decades) no planned satellite mission fulfilling the requirements in terms of resolution and/or  
301 acquisition repetitiveness for the proposed monitoring application as discussed below.

### 302 ***2.3. Temporal scales***

303 CO<sub>2</sub> injection operations are typically planned to last between 25 and 50 years. This “long  
304 term” monitoring implies considering several issues.

305 A first difficulty is the availability of a space-borne sensor, whose mission durations are  
306 typically of the order of a ten of years (e.g. see Hanssen, 2005, Table 2). Thus, any long term  
307 monitoring of the injection operations should be designed potentially considering a minimum  
308 of 2 to 3 satellites, whose characteristics (orientation of the orbital trajectory, center  
309 frequency, C-, L- band, etc.) might change from a satellite to another and not be necessarily  
310 suited for interferometric analysis. For instance, the currently-used ENVISAT mission, which  
311 was deeply modified in October 2010 (change in the orbital characteristics, affecting the  
312 possibility of carrying out reliable PSI processing after this event), will come to an end in the  
313 coming years. A transition period with another space-borne sensor should be accounted for in  
314 the design of long term monitoring plan. For instance, the successor of ENVISAT, namely  
315 Sentinel 1, is to be launched in 2013. This 7-12 years mission will consist in a space-borne

316 SAR in C-band (and therefore providing data similar to ASAR) with a repetitiveness of 12  
317 days. Considering an ideal data-set for PSI baseline of >30 images the transition period  
318 should last ~10 months, i.e. before the planned commercial-scale deployment of storage sites  
319 by 2020 (IEA, 2009).

320 A second difficulty arises from the decorrelation of PS over time, i.e. the “life expectancy” of  
321 the PS over such long time durations. Ferreti et al. (2003) tackled this issue by identifying  
322 points corresponding to PS only on sub-sets of the full ESA-ERS data set over the period  
323 1992-2003 on the Milano urban area. This consisted in identifying PS, which have appeared  
324 or have disappeared during a given time span between the first and last acquisition. The  
325 number of such points is usually 10% of the number of PS over a period of a ten of years.  
326 This can be considered an order of magnitude of the life expectancy of a PS.

327 Though requiring further investigations, the effect of the land cover nature (urban / rural) is  
328 expected to have little influence on the life expectancy of PS. It is true that on vegetated area  
329 the temporal decorrelation (on none-PS points) is globally higher than on urban areas, but  
330 pure point target PS are little affected by temporal decorrelation (as they are identified by the  
331 temporal stability of their signal) whatever on urban and on non-urban areas.

332 The use of high resolution data is expected to improve the life expectancy of PS. As shown by  
333 Crosetto et al. (2010), higher PS densities are expected with higher resolution sensors.  
334 Assuming an equivalent PS decay rate for different resolutions, the total number of PS is  
335 expected to be larger with high resolution sensors considering an isolated small area with high  
336 PS density located in a larger area depleted of PS (e.g. small groups of buildings in a larger  
337 agricultural zone). Following this reasoning, the probability of having at least a few PS lasting  
338 during the whole observation period is therefore higher with high resolution sensors (provided  
339 that a maximum of isolated building groups will keep some PS during the observation  
340 period). Yet, as mentioned in section 2.2, the high resolution requirement is limited by the

341 large swath requirement. Current sensor TerraSAR-X (Strip Map Mode) and future Sentinel-1  
342 mission should both fulfill such a trade-off, but with major differences in the data provision  
343 policy.

344 This latter issue should be carefully accounted for, because long term monitoring possibly  
345 implies constituting a large data base (depending on the acquisition and processing frequency;  
346 which is further discussed in section 2.4). To remain cost-effective regarding ground-based  
347 geodetic measurement techniques (e.g., optical levelling, GPS, tiltmeters, etc.), a possible  
348 strategy can be similar to the provision policy associated to the Global Monitoring for  
349 Environment and Security (<http://www.gmes.info/>), which allows obtaining the data at low  
350 price as envisaged for the future Sentinel-1 mission. The interested reader can refer to (Rucci  
351 et al., 2012) for additional discussions on the use of future Sentinel-1 and new X-band sensors  
352 for reservoir applications.

#### 353 ***2.4. Spatio- temporal evolution***

354 The monitoring of CO<sub>2</sub> storage sites has two major objectives (see e.g., Benson, 2006). A first  
355 objective, categorized as “verification”, focuses on the monitoring of the expected behaviour  
356 of the storage complex, in particular detecting the location and quantifying the size of CO<sub>2</sub>  
357 plume within the reservoir and tracking the pressure front propagation. The second objective,  
358 categorized as “early-warning”, focuses on the detection of any “abnormal behaviour”, i.e.  
359 deviations from the expected behaviour of the storage complex. This latter case corresponds  
360 to the occurrence of unwanted events such as the sudden (i.e. over a short time span) multi-  
361 millimetric uplift localized on a fault zone, which may be related to the fault reactivation at  
362 depth (see e.g., Rutqvist et al., 2010).

363 Regarding the “verification” objective, the acquisition and processing rate should be chosen  
364 based on the simulations of the expected spatio- temporal evolution of the deformation  
365 phenomenon. In this view, section 1 provides useful orders of magnitude for a typical

366 injection scenario. At a given location, Figure 2 shows that the deformation phenomenon is  
367 characterized by a highly non-linear evolution over time. This might limit the performance,  
368 because the PSI technique is generally better applied for rather conservative types of  
369 deformation (e.g. Hanssen, 2005), e.g., characterized with (approximately) uniform  
370 deformation velocity relatively linear temporal evolution of deformation velocity or periodic  
371 (such as seasonal natural gas storage, Teatini et al., 2011). To tackle this issue, an alternative  
372 would be to focus on the discrepancies of the measured displacement field respect to the  
373 proposed evolution model, i.e. deviation to the predictive model. By subtracting the model-  
374 based simulation of the phase to the interferometric data, an important part of the (non-linear)  
375 temporal signal would be removed, facilitating the PSI processing (in particular by reducing  
376 the risk of unwrapping errors). Besides, the important information is the (unforeseen)  
377 discrepancy respect to the model that is needed for adjusting the representation of the  
378 phenomenon. The proposed iterative procedure described in section 3.3 that revisits  
379 periodically the knowledge of the phenomenon, could partly deal with this issue.

380 Figure 1B provides information on the spatio- temporal evolution of the “deformation front”  
381 given a typical injection scenario (see details in section 1.2). An individual measurement point  
382 located at a given lateral distance from the injection zone, requires a major and more  
383 frequently sampled monitoring during a specific period of the order of ~2-4 years, the  
384 beginning of this period depending on the distance to the injector. In other terms, a  
385 “deformation front”, as schematically depicted in Figure 4, affects the location during this  
386 short time span  $\Delta t=2-4$  years. Before the front has passed no deformation affects the point.  
387 After, the point has smaller displacement (see Fig. 4). Such a spatio- temporal behaviour has  
388 implications on both the choice of the frequency of image data acquisition (i.e. sampling  
389 procedure) and of the processing rate (i.e. frequency of PSI analysis).

390 At a given location, the monitoring should be highly-rated sampled during the short period of  
391 the deformation front passage. As indicated in section 2.1, >30 images is an ideal data set size  
392 for precision reasons. The orbit cycle of ASAR-like sensors (about 10 acquisitions per year)  
393 may be therefore insufficient to carry out such a measurement at the limit of the sensitivity of  
394 the method. Current sensor TerraSAR-X (Strip Map Mode) and future Sentinel-1 mission  
395 should fulfill such a requirement (with both repetitiveness of the order of a ten of days), but  
396 with differences in the data provision policy (see section 2.3).

397 Besides, changes in the velocities values of the differential displacements are expected to be  
398 detectable only after a few months (except for the case of multi- millimetric sudden ground  
399 movements, which is discussed in the following). The processing of the data image with very  
400 high frequency (e.g. every day) may not be appropriate given the described physical evolution  
401 of the deformation, but also considering cost and resource constraints. Considering the  
402 expected spatio- temporal evolution of the deformation phenomenon as calculated for the  
403 typical injection scenario described in the section 1.2, one PSI analyse every 3 – 6 months can  
404 be proposed to fulfil the “verification” objective of monitoring. Noteworthy, this processing  
405 rate is intermediate between quasi- real time (e.g. bottom-hole fluid pressure) and pluri-  
406 annual monitoring techniques (e.g. seismic campaign).

407 Regarding the “early- warning” objective of the monitoring, two cases can be considered. On  
408 the one hand, potential zones at risk (e.g. fault zones, injection zone, etc.) can be identified  
409 prior the injection operations based on a risk assessment procedure (see Bouc et al., 2011). On  
410 these localized zones, a specific PSI analysis can be envisaged using high resolution/high  
411 repetitiveness (but reduced swath) data equivalent to those provided by the current X-band  
412 sensors TerraSAR-X or COSMO-SkyMed (see e.g., Ferretti et al. 2011b), to complement the  
413 PSI analysis for the “verification” monitoring. Noteworthy, other ground-based geodetic

414 techniques would require systematic on-site measurements, such an approach being time  
415 consuming and resource intensive.

416 On the other hand, if any “abnormal behavior” is detected in an “un-expected” zone either  
417 after processing the image data or based on other indicators (induced seismicity recorded at  
418 the surface due to possible fault reactivation; increase of the fluid pressure recorded in the  
419 monitoring aquifer indicating a possible leakage, etc.), the considerations for data acquisition  
420 and processing rate as discussed for the verification monitoring should be adjusted. The great  
421 advantage of PSI analysis compared to ground-based geodetic measurement is the possibility  
422 to assess deformation after the unwanted event has occurred, because image data would have  
423 been archived without user’s intervention (e.g., every 12 days using the future Sentinel-1  
424 sensor). Punctual and local studies on short time spans can also be proposed to focus on the  
425 “un-expected” zone at risk to complement the PSI analysis for the verification monitoring.

426 *[Figure 4 about here]*

### 427 **3. Planning a network of artificial reflectors**

#### 428 ***3.1. Description of corner reflector devices***

429

430 One major difficulty to the implementation of PSI in the CO<sub>2</sub> storage context stems from the  
431 potentially low PS density over such large areas as previously discussed. Though improved  
432 co-registration and use of more efficient computational techniques (the interested reader can  
433 refer to Sousa et al., 2011) can provide valuable support, a potential solution to enhance the  
434 performance in regions where bright man-made structures are merely absent can rely on the  
435 installation of artificial PS, i.e. corner reflectors CR (e.g., Novali et al., 2005). These artificial  
436 metallic devices (of generally trihedral or cubic geometry characterized by a few tens of  
437 centimeters long) are installed on ground providing high backscatter to the radar signal to

438 complement the existing “natural” PS network, i.e. to fill the gap between natural persistent  
439 reflectors. This approach has been proposed in other contexts (mine, volcano, coastland and  
440 marshland environments, etc.), where the ground movements’ detection has proved to be very  
441 challenging. See for instance the recent application case in the Venice lagoon (Teatini et al.,  
442 2010).

### 443 ***3.2. Optimizing the position of the CR***

444 To the authors’ knowledge, very few works have handled the issue of planning the position of  
445 CR in a predictive fashion, i.e. before any ground deformation measurement has been carried  
446 out. For instance, in the recent interferometric analysis of the land subsidence in the Venice  
447 lagoon (Teatini et al., 2010), a network of 55 CR has been planned taking into account a fixed  
448 distance of 1 km between them of any adjacent natural reflectors. Yet, these were installed  
449 only once the full interferometric analysis had been carried out for a ten of years.

450 Planning the CR network using an “one-size-fits-all” approach, i.e. using a fixed distance  
451 value may rapidly become impracticable considering the large area expected at the end of  
452 injection (of ~325 km<sup>2</sup> after 25 years for the case modeled in section 1.3). Optimizing the  
453 location of the CR should result from a trade-off between the issues related to the installation  
454 of such devices (costs, authorizations, maintenance, etc.) and the requirements in terms of  
455 coverage and precision for the PSI results. Furthermore, the time-scales of CO<sub>2</sub> storage  
456 constitute a major constraint for the monitoring plan that should be designed to follow the  
457 long term evolution of the ground movement over a time span ranging from 25 to 50 years.

458 An example of a ground-based network, i.e. of devices fixed at the surface that exist over such  
459 a long time duration, is provided by the networks of benchmarks used for national spatial  
460 reference systems (e.g. in France, the currently-used network has been installed since the 19<sup>th</sup>  
461 century), but dimensions of such ground-based devices have nothing comparable to the ones  
462 of a CR.

463 In this context, a crude design approach based on the expected surface deformation calculated  
464 regarding the whole time duration of the storage project may be highly limited by both  
465 maintenance issues of the CR network given such large spatio-temporal scales and by the  
466 changes in the sensors characteristics (typically each 7-10 years, see section 2.2) over the full  
467 lifecycle of the storage injection phase. Therefore, we advocate a design strategy thought in  
468 an iterative fashion:

469

- 470     ▪ *Step1*: estimate the expected spatio-temporal evolution of ground surface  
471         displacements induced by CO<sub>2</sub> injection operations at different epochs for the full  
472         period of injection. The duration of each epoch should be no longer than a ten of years  
473         to handle the possible change in the sensors characteristics. Let us consider the  
474         estimates of the surface deformation after 5 epochs of 10 years each. This step should  
475         be based on large-scale geomechanical analysis of the complex site. This can rely on  
476         analytical models such as the multilayered visco-elastic solution developed by Fokker  
477         and Orlic (2006) or in a first approach, the one described in section 1 presenting the  
478         attractive feature of a rapid estimation, but limited by the simplifications inherent to  
479         the analytical nature of the model of such a simplified model (as discussed in section  
480         1.3). A more sophisticated analysis can rely on large-scale coupled numerical models  
481         as demonstrated by Rutqvist et al. (2010) in the In Salah's context. The advantage of  
482         such analysis are the ability to take into account complex injection scenarios, complex  
483         reservoir pore pressure spatio-temporal evolution, complex geological structures (e.g.,  
484         multi-layered system as present in sedimentary basin suitable for CO<sub>2</sub> storage,  
485         Birkholzer et al., 2009;
- 486     ▪ *Step2*: based on the expected extent of detectable deformation surface, localize the a  
487         priori good candidate for PS, i.e. spatial points that appear to be persistent in the

488 present, but above all, that shall remain persistent over the full duration of the  
489 injection. Long term “natural” PS can constitute man-made structures within urban  
490 zones (historical monuments, churches, industrial plants, roads, etc.). We can consider  
491 that a large number of these spatial points identified as PS will keep their  
492 characteristics (reflectivity) over the time duration of the considered epoch (of a ten of  
493 years). This assumption can be considered valid regarding the study of Ferreti et al.  
494 (2003), as discussed in section 2.2.⇨

495 ■ *Step3*: optimize the position of the corner reflectors CR considering the expected  
496 detectable surface deformation for the whole duration of the injection. We advocate  
497 choosing the distance between CR and natural PS based on a criterion dependent on  
498 the initial network of natural PS. The idea is to maximize the spatial coverage of the  
499 area where ground deformation is expected to be detected considering the location of  
500 identified potential “natural” PS. Formally, this can be achieved by treating the  
501 “natural” persistent scatters as Voronoi sites and by affecting to each of them a  
502 Dirichlet cell (also named Voronoi cell) consisting of all points closer to PS than to  
503 any other site as schematically depicted in Figure 6A. The segments of Voronoi cell  
504 are all the points in the space that are equidistant to the two nearest sites PS. The  
505 potential positions of the CR are then chosen as the Voronoi nodes corresponding to  
506 the equidistant to three (or more) PS sites. The positions of the CR merely derive from  
507 a pure mathematical space-filling criterion, but in real-case applications, adjustments  
508 will certainly be necessary if the Voronoi-based method indicates installing the CR in  
509 densely vegetated cover (forests, wetlands, etc.), which may highly prevent the  
510 detection or the installation of the CR, or too close to another CR (e.g., with a distance  
511 <1 km). Then, the CR only lying within the expected detectable zone for the

512 considered 10-years epoch, can be selected. These CR should be installed to help  
513 monitoring the expected surface deformation over the duration of one epoch.

514 Based on the discussions in section 2, the PSI analysis to fulfil the “verification” objective of  
515 the monitoring can be conducted using data characterized by a large swath, a rather good  
516 resolution and repetitiveness of a ten of days. The processing rate of the image data should be  
517 chosen depending on the simulation predictions for the spatio- temporal evolution of the  
518 deformation phenomenon associated with CO<sub>2</sub> injection. The simulations for the typical  
519 injections scenario (section 1.2) show that a processing of 3-6 months can be envisaged  
520 during the 10-year epoch. This rate can be adjusted especially depending on the detection of a  
521 sudden “abnormal behaviour” on a localized zone (e.g., sudden multi- millimetric uplift due  
522 to possible fault reactivation). A complementary PSI analysis using high resolution / high  
523 repetitiveness (but reduced swath) data can be proposed on these zones at risk (see discussion  
524 in section 2.4). Such an iterative approach allows a frequent re-interpretation of the  
525 discrepancies between model and measurements in terms of evolution predictions (i.e.  
526 deviation to the predictive model). Valuable information on the storage complex behaviour  
527 can be extracted in an inversion procedure as proposed more specifically in the field of CO<sub>2</sub>  
528 storage by Vasco et al. (2008a&b). The combination of both information (correction of the  
529 model based on the measurements and inversion of the complex behavior) can serve to  
530 increase the quality and robustness of the predictions.

531 The procedure is then repeated for the next 10-years epochs (step 1). Using the initial PS  
532 network enriched with the CR identified for the previous epoch (step 2), the next CR (i.e.  
533 necessary for monitoring the next epoch) can be identified using the updated expected  
534 detectable surface deformation region (step 3), and the procedure is then repeated.

535 ~~Noteworthy,~~ Before the end of each 10-years observation epoch, a transition period should be  
536 envisaged between two successive satellite missions, with sensors of possibly different

537 characteristics. During this period, a sufficient amount of SAR data (> 30 images) should be  
538 acquired for the PSI baseline using the new sensor. Considering a repetitiveness of a ten of  
539 days, this period should last ~1 year. Figure 5 summarizes the sequence of the steps  
540 considering two epochs and two different sensors.

541 *[Figure 5 about here]*

542 In case of sensors with different characteristics, a change in the configurations (e.g.  
543 orientation) of the CR, which have been installed during the first epoch, should be envisaged  
544 to make these CR “visible” by the new sensor. In such a case, a gap in the produced  
545 deformation time series may be expected of the order of few months, but only partly on the  
546 ground surface covered by the SAR data, i.e. corresponding to the region whose CR were  
547 adapted to the first 10-years epoch. To the authors’ knowledge, the transition between two  
548 sensors during the implementation of SAR interferometry combined with CR has not been  
549 experienced yet and requires further investigations.

550 Finally, considering such a long term monitoring, the possibility that during certain periods,  
551 the lack of satellite mission with suitable characteristics cannot be fully discarded. In such a  
552 case, the information provided before and after the information gap could still provide useful  
553 information on the evolution of the injection processes.

### 554 ***3.3. Application to a potential storage site in the Paris basin***

555 To illustrate the main steps of the proposed methodology, we apply the described  
556 methodology to a potential injection site selected within the PICOREF sector in the Paris  
557 basin (Figure 6). This potential storage site was identified based on the combination of criteria  
558 in terms of capacities and injectivity, environmental constraints, existing land-use and  
559 underground-use, economic and social aspects and based on a comprehensive risks analysis  
560 (Grataloup et al., 2008; Bouc et al., 2011). Figure 6 shows the location of the potential  
561 injection well (outlined by a red cross marker). We consider 40 years of CO<sub>2</sub> injection at a

562 rate of 2 Mt/y into the 1500m deep carbonate aquifer of the Dogger formation. The aquifer  
563 properties are: intrinsic permeability of  $1.10^{-13}$  m<sup>2</sup>; porosity of 12 %; Young's modulus of 24  
564 GPa; Poisson's ratio of 0.29 (Rohmer and Seyedi, 2010 and references therein).

565 *[Figure 6 about here]*

- 566     ▪ *Step 1:* in this example, the analytical model described in section 1 is used to estimate  
567 the lateral extent of the expected detectable zone of vertical displacements  
568 (considering a 5 mm detection threshold) induced by a whole CO<sub>2</sub> injection duration  
569 of 40 years and considering four 10-years long epochs. The final zone represented by a  
570 black circle in Figure 6 covers a total area of ~220 km<sup>2</sup> and corresponds to the zone of  
571 maximum extent that should be monitored by the PSI technique over the whole life  
572 span of the potential storage site;
- 573     ▪ *Step 2:* we consider each centroids of the urban zone present within the detectable  
574 zone for the whole injection duration (total number of 24 zones). These represent  
575 localized zones where good candidates for natural PS are highly likely to be detected.  
576 In a preliminary approach, we only consider these centroids as natural PS (outlined in  
577 Figure 7 as pink diamond markers);
- 578     ▪ *Step 3:* on this basis, we assign to each of the centroids a Voronoi cell (Figure 7A) and  
579 choose the potential CR as the Voronoi cells (outlined in Figure 7A as blue triangular  
580 markers); the CR lying within forest zones or distant from each other of less than 1km  
581 are detected and are re- adjusted (deleted or re-localized). A total number of 23 CR are  
582 in this manner identified within the detectable region for the whole duration of the  
583 injection (here 40 years, black -coloured circle in Figure 7B).

584 *[Figure 7 about here]*

585 Using the region of detectable deformation for the first 10 years of injection (light grey-  
586 coloured circle in Figure 7B), a total of 6 CR are identified through the Voronoi analysis.

587 Among the identified CR, two CR should be re- localized, because they lie within forest areas  
588 and one CR should be deleted, because it is too close from the others. Without any other  
589 consideration (such as legal issues, accessibility of the site, ...), we are able to propose a  
590 monitoring procedure adapted to the expected characteristics of the deformation for the first  
591 10 years of injection both based on CR-InSAR and on current PSI techniques.  
592 For the next 10-years epoch, Figure 8 provides an illustration of the location of the  
593 corresponding CR (i.e. after 10 years of injection) using the original PS network (Figure 7A,  
594 pink coloured diamond markers) enriched with the 5 CR selected for the first 10-years epoch.  
595 The expected detectable regions for the whole injection duration (at 20, 30 and 40 years) are  
596 then re- estimated (step 1), here assumed unchanged for illustration purposes. On this basis,  
597 the CR for the whole duration are identified (step 2 & 3). Then, using the expected detectable  
598 deformation region for the next 10-years epoch (here for the date 20 years), the CR for this  
599 epoch are selected (Figure 8B).

600 *[Figure 8 about here]*

#### 601 **4. Concluding remarks and recommendations**

602 The present paper proposes a description of the characteristics of the surface deformation,  
603 which will be expected during the injection of CO<sub>2</sub> into deep aquifers during 25 – 50 years.  
604 On this basis, the associated constraints for the planning of a monitoring plan relying on PSI  
605 techniques are discussed. To overcome such limitations, we focused on the optimisation of a  
606 CR (corner reflectors) network. An iterative strategy is proposed, which is justified by the  
607 large spatial extent of the expected detectable region and by the changes in the sensors  
608 characteristics (typically each 7-10 years) that could result in a need of re-organisation of the  
609 network (and even CR characteristics such as orientation). At each period (say, every 10  
610 years), the number and location of the CR, necessary for the monitoring of the surface

611 deformation of the next epoch, are estimated based on the prediction of surface deformation  
612 using large-scale geomechanical models. Furthermore, we propose to focus on discrepancies  
613 between model and measurements, which can be useful in terms of evolution predictions. To  
614 fulfil the “verification” objective of the monitoring, the PSI analysis should be frequently  
615 conducted during each epoch with a processing rate, which should be chosen depending on  
616 the predicted spatio- temporal evolution of the deformation phenomenon. The simulation  
617 results for a typical injection scenario show that a processing rate of the order of a few months  
618 may be sufficient. Such a frequent re-examination of the situation and model correction is  
619 therefore useful in a perspective of forecasting consequences of the injection. To fulfil the  
620 “early-warning” objective of the monitoring, a complement should be envisaged so that well  
621 definite zones at risk (such as fault zones) should be monitored using high repetitiveness /  
622 high resolution (but reduced swath) data. In both cases, a careful attention should be paid to  
623 cost and resource issues especially regarding provision policies of image data.

624 Finally, from now to the start of injection and during the 50 years injection, improvement of  
625 PSI processing techniques can occur. For instance, Ferretti et al. (2011a), recently proposed a  
626 technique (SqueeSAR<sup>TM</sup>) based on the concept of diffuse scatterers, which can improve  
627 considerably the density of usable “natural” scatterers on certain un-urbanised area. See the  
628 recent application of such a technique at In-Salah (Rucci et al., 2012). If such improvement is  
629 efficient for surface characteristics such as those existing on the monitored area, an  
630 optimisation of the network could be proposed – probably based on a reduced CR number.

631 The periodic re-thought of the CR network will therefore allow the possibility of  
632 methodological improvement in addition to taking into account new sensors characteristics.

633

## 634 **Acknowledgements**

635 This work was funded under the BRGM's Directorate of Research project. We also thank  
636 Marcello de Michele for useful discussions.

637

## 638 **Appendix A: General solution to ground displacements**

639 Segall and co-authors (Segall, 1992; Segall and Fitzgerald, 1998) have presented poro-elastic  
640 solutions for stress and displacement fields estimate in an elastic half-space, induced by fluid  
641 extraction (or injection, the solutions being merely the opposite) for general axi-symmetric  
642 geometries with arbitrary pressure radial distribution within the reservoir (given as a function  
643 of space and time for instance from field data and/or reservoir simulations). Noteworthy this  
644 solution provides both horizontal and vertical surface displacements, but we will focus on the  
645 latter one.

646 The variation in reservoir pore pressure  $p$  is assumed to mainly govern the volumetric strain in  
647 the reservoir. The vertical displacement at the radial distance  $r$  at the free surface  $u_z(r)$  results  
648 from the cumulative contribution of all the rings of dilatation at radius  $\tilde{r}$  and depth  $Z$  (as  
649 schematically depicted in Figure 9), the magnitude of dilation being proportional to the  
650 product of the pressure  $p$  and of the Biot's coefficient  $b$ . Based on the Green's function at the  
651 free surface  $g_z(r)$  for the radially symmetric case (Equation A1b), the solution for  $u_z(r)$  holds  
652 as follows:

653

$$u_z(r) = \frac{b \cdot 2(1 + \nu)}{E} \int_0^{\infty} \int_0^{\infty} p(\tilde{r}, Z) \cdot g_z(r, z, \tilde{r}, Z) d\tilde{r} dZ \quad (\text{A1})$$

654  
655

656 where:

657

$$g_z(r) = (1 - 2 \cdot \nu) \cdot \tilde{r} \cdot \frac{Z \cdot K^3 \cdot F(K)}{4\pi \cdot (1 - K^2) \cdot (\tilde{r} \cdot r)^{3/2}} \quad (\text{A2})$$

658  
659

660 where:

661

662  $K^2 = 4 \cdot r \cdot \tilde{r} / (\tilde{r} + r)^2 + Z^2$  and  $F(K)$  is the complete elliptic integral of the second kind.

663 The physical properties are described in Table 1.

664

665 *[Figure 9 about here]*

666

## 667 **Appendix B: General solution to the pressure build-up**

668 The radial pore pressure  $p(r, t)$  evolution (Equation B1) is assessed based on the analytical

669 solution developed by Mathias et al. (2009a) using the method of matched asymptotic

670 expansions for the non-inertial flow of CO<sub>2</sub> into a slightly compressible brine aquifer

671 (assumed to be an open system, and the pressure corresponds to the initial one) with a vertical

672 pressure equilibrium assumption. This solution holds as follows, distinguishing three zones:

673 - the CO<sub>2</sub> fully saturated zone (near the injector), for  $x \leq 2\gamma$  ( $x$  being dependent on  $r$ , see

674 Eq. B2 and  $\gamma$  is the ratio of the viscosity of CO<sub>2</sub>  $\mu_{\text{CO}_2}$  to the one of the brine  $\mu_{\text{brine}}$ );

675 - the diphasic zone (brine + CO<sub>2</sub>), for  $2\gamma \leq x \leq 2/\gamma$ ;

676 - the brine-filled zone in the far field for  $2/\gamma \leq x$ .

677

$$\begin{aligned}
p(x,t) = & \frac{1}{2\gamma} Ei\left(\frac{\alpha \cdot x}{4 \cdot \gamma}\right) + \frac{1}{2\gamma} \left( \ln\left(\frac{\alpha \cdot x}{4 \cdot \gamma}\right) + \kappa \right) \\
& + \begin{cases} -\frac{1}{2} \ln\left(\frac{x}{2 \cdot \gamma}\right) - 1 + \frac{1}{\gamma} - \frac{1}{\gamma} \left( \ln\left(\frac{\alpha}{2 \cdot \gamma^2}\right) + \kappa \right) & \text{if } x \leq 2\gamma \\ -\left(\frac{x}{2 \cdot \gamma}\right)^{0.5} + \frac{1}{\gamma} - \frac{1}{2\gamma} \left( \ln\left(\frac{\alpha}{2 \cdot \gamma^2}\right) + \kappa \right) & \text{if } 2\gamma \leq x \leq 2/\gamma \\ -\frac{1}{2\gamma} \left( \ln\left(\frac{\alpha \cdot x}{2 \cdot \gamma}\right) + \kappa \right) & \text{if } x \geq 2/\gamma \end{cases}
\end{aligned} \tag{B1}$$

678  
679

680 where:

681

$$\begin{aligned}
x = & \frac{(r/r_w)^2}{t \cdot Q_w / (2\pi \cdot \omega \cdot H \cdot (r_w)^2 \cdot \rho_{CO_2})} \\
\alpha = & \frac{Q_w \cdot \mu_{CO_2} \cdot (c_{rock} + c_{brine})}{2\pi \cdot H \cdot k}
\end{aligned} \tag{B2}$$

682  
683

684 where:

685  $\kappa \approx 0.5772$  is Euler-Mascheroni constant ;  $r_w$  is the injector well radius (m);  $\rho_{CO_2}$  is the CO<sub>2</sub>  
686 density (kg/m<sup>3</sup>);  $Q_w$  is the mass injection rate (kg/s);  $t$  time (s);  $c_{brine}$  is the brine  
687 compressibility (Pa<sup>-1</sup>); Other parameters are described in Table 1. Fluid properties are derived  
688 (viscosity, density and compressibility for both brine and CO<sub>2</sub>) based on the empirical  
689 correlations with pressure and temperature supplied by Mathias et al. (2009b).

690

691 **References**

- 692 Bouc, O., Bellenfant, G., Dubois, D., Guyonnet, D., Rohmer, J., Wertz, F., Gastine, M.,  
693 Jacquemet, N., Vong, C. Q., Grataloup, S., Picot-Colbeaux, G., Fabriol, H., 2011.  
694 Safety criteria for CO<sub>2</sub> geological storage: Determination workflow and application in  
695 the context of the Paris Basin. *Energy Procedia* 4, 4020-4027.
- 696 Bell, J. W., Amelung, F., Ferretti, A., Bianchi, M., Novali, F., 2008. Permanent scatterer  
697 InSAR reveals seasonal and long-term aquifer-system response to groundwater  
698 pumping and artificial recharge. *Water Resour. Res.* 44, W02407,  
699 doi:10.1029/2007WR006152.
- 700 Benson, S.M., 2006. Monitoring Carbon Dioxide Sequestration in Deep Geological  
701 Formations for Inventory Verification and Carbon Credits. *Proceedings of the SPE*  
702 *Annual Technical Conference and Exhibition*, San Antonio, Texas, U.S.A., 24-27  
703 September 2006, SPE Paper no. 102833.
- 704 Birkholzer, J. T., Zhou Q., Tsang C.-F., 2009. Large-scale impact of CO<sub>2</sub> storage in deep  
705 saline aquifers: A sensitivity study on pressure response in stratified systems. *Int. J.*  
706 *Greenhouse Gas Control* 3(2), 181-194.
- 707 Colesanti, C., Ferretti, A., Locatelli, R., Novali, F. and Savio, G., 2003. Permanent Scatterers:  
708 Precision Assessment and Multi-platform Analysis. *IEEE International Symposium on*  
709 *Geoscience and Remote Sensing (IGARSS)*, Toulouse, France, July 21-25, 1193 –  
710 1195.
- 711 Crosetto, M., Monserrat, O., Iglesias, R. and Crippa, B., 2010. Persistent Scatterer  
712 Interferometry: Potential, Limits and Initial Cand X-band Comparison.  
713 *Photogrammetric Engineering and Remote Sensing* 76(9), 1061-1069.

714 European Commission (EC), 2009. Directive 2009/31/EC of the European Parliament and of  
715 the Council of 23 April 2009 on the geological storage of carbon dioxide and  
716 amending Council Directive 85/337/EEC, European Parliament and Council  
717 Directives 2000/60/EC, 2001/80/EC, 2004/35/EC, 2006/12/EC, 2008/1/EC and  
718 Regulation (EC) No 1013/2006;2009.

719 Ferretti, A., Prati, C., Rocca, F., 2000. Nonlinear subsidence rate estimation using permanent  
720 scatterers in differential SAR interferometry. *IEEE Trans. Geosci. Remote Sens.*  
721 38(5), 2202–2212.

722 Ferretti, A.; Colesanti, C.; Perissin, D.; Prati, C.; Rocca, F. Evaluating the Effect of the  
723 Observation Time on the Distribution of SAR Permanent Scatterers. Proceedings of  
724 the FRINGE 2003 Workshop (ESA SP-550). ESA/ESRIN, Frascati, Italy, 1-5  
725 December 2003. Editor: H. Lacoste. Published on CDROM., p.26.1

726 Ferretti, A.; Fumagalli, A., Novali, F., Prati, C.; Rocca, F., Rucci, A. 2011a. A New  
727 Algorithm for Processing Interferometric Data-Stacks: SqueeSAR, *IEEE Transactions*  
728 *on Geoscience and Remote Sensing* 49(9), 3460 – 3470.

729 Ferretti, A., Tamburini, A., Novali, F., Fumagalli, A., Falorni, G., Rucci, A. 2011b. Impact of  
730 high resolution radar imagery on reservoir monitoring. *Energy Procedia* 4, 3465–3471.

731 Fokker, P.A., Orlic, B., 2006. Semi-analytic modeling of subsidence. *Math. Geol.* 38, 565–  
732 589.

733 Grataloup, S., Bonijoly, D., Brosse, E., Dreux, R., Garcia, D., Hasanov, V., Lescanne, M.,  
734 Renoux, P., Thoraval, A., 2009. A site selection methodology for CO<sub>2</sub> underground  
735 storage in deep saline aquifers: case of the Paris Basin. *Energy Procedia* 1(1), 2929-  
736 2936.

737 Hanssen, R. F., 2005. Satellite radar interferometry for deformation monitoring: a priori  
738 assessment of feasibility and accuracy. *International Journal of Applied Earth*  
739 *Observation and Geoinformation* 6, 253–260, doi:10.1016/j.jag.2004.10.004.

740 Hettema, M., Papamichos, E., Schutjens, P., 2002. Subsidence delay: Field observations and  
741 analysis, *Oil Gas Sci. Technol.* 57, 443–458.

742 International Energy Agency (IEA), 2009. *Technology Roadmap – Carbon Capture and*  
743 *Storage*, IEA, Paris, 46 p.

744 IPCC (Intergovernmental Panel on Climate Change), 2005. *IPCC Special Report on Carbon*  
745 *Dioxide Capture and Storage*. Cambridge University Press, New York, USA.

746 Mathias, S.A., Hardisty, P., Trudell, M., Zimmerman, R., 2009a, Approximate Solutions for  
747 Pressure Buildup During CO<sub>2</sub> Injection in Brine Aquifers. *Transport in Porous Media*  
748 79, 265-284.

749 Mathias, S.A., Hardisty, P.E., Trudell, M.R., Zimmerman, R.W., 2009b, Screening and  
750 selection of sites for CO<sub>2</sub> sequestration based on pressure buildup. *International*  
751 *Journal of Greenhouse Gas Control* 3(5), 577-585.

752 Mathieson, A., I. Wright, D. Roberts, and P. Ringrose (2009), Satellite imaging to monitor  
753 CO<sub>2</sub> movement at Krechba, Algeria. *Energy Procedia* 1(1), 2201–2209.

754 Mobach, E., Gussinklo, H.J., 1994. In situ reservoir compaction monitoring in the Groningen  
755 field. *Proceedings of EUROCK94 Rock Mechanics in Petroleum Engineering*, 29-31  
756 August 1994, Delft, Netherlands.

757 Novali, F., Ferretti, A., Prati, C., Rocca, F., Savio, G., Musazzi, S., 2005. PSInSAR  
758 Validation by Means of a Blind Experiment Using Dihedral Reflectors. *Proceedings of*  
759 *FRINGE 2005*, Frascati, Italy, 28 November– 2 December 2005, available also online:  
760 <http://earth.esa.int/workshops/fringe2005/proceedings/>.Novali et al., 2005.

761 Raucoules, D., Colesanti, C., Carnec, C., 2007. Use of SAR interferometry for detecting and  
762 assessing ground subsidence. *Compte Rendus Geosciences* 339(5), 289-302.

763 Raucoules, D., Bourguine, B., de Michele, M., Le Cozannet, G., Closset, L., Bremmer, C.,  
764 Veldkamp, H., Tragheim, D., Bateson, L., Crosetto, M., Agudo, M., Engdahl, M.,  
765 2009, Validation and Intercomparison of Persistent Scatterers Interferometry: PSIC4  
766 project results. *Journal of Applied Geophysics* 68(3), 335-347.

767 Rohmer J., Seyedi D., 2010. Coupled large scale hydromechanical modelling for caprock  
768 failure risk assessment of CO2 storage in deep saline aquifers. *Oil & Gas Science and*  
769 *Technology - Rev. IFP* 65(3), 503-517.

770 Rucci, A., Ferretti, A., Monti Guarnieri, A., Rocca, F., 2012. Sentinel 1 SAR interferometry  
771 applications: The outlook for sub millimeter measurements. *Remote Sensing of*  
772 *Environment* 120, 156–163.

773 Rutqvist, J., Vasco, D. W., Myer, L., 2010. Coupled reservoir-geomechanical analysis of CO2  
774 injection and ground deformations at In Salah, Algeria. *International Journal of*  
775 *Greenhouse Gas Control* 4(2), 225-230.

776 Segall, P., 1992. Induced Stresses due to Fluid Extraction from Axisymmetric Reservoirs.  
777 *Pageoph.* 139(3/4).

778 Segall, P., Fitzgerald, S. D., 1998. A note on induced stress changes in hydrocarbon and  
779 geothermal reservoirs. *Tectonophysics* 289, 117–128.

780 Singh, M. M., 1992. Mine subsidence. *SME Mining Engineering Handbook*, in: Hartman,  
781 H.L. (Ed), Society for mining metallurgy and exploration, Inc., Littleton, Colorado,  
782 USA, pp. 938-971.

783 Sousa, J.J., Hooper, A. J., Hanssen, R. F., Bastos, L. C., Ruiz, A. M., 2011. Persistent  
784 Scatterer InSAR: A comparison of methodologies based on a model of temporal

785 deformation vs. spatial correlation selection criteria. *Remote Sensing of Environment*  
786 115, 2652–2663.

787 Tamburini, A., Bianchi, M., Giannico, C., Novali, F., 2009. Retrieving surface deformation  
788 by PSInSAR™ technology: A powerful tool in reservoir monitoring. *International*  
789 *Journal of Greenhouse Gas Control* 4(6), 928-937, doi:10.1016/j.ijggc.2009.12.009.

790 Teatini, P., Castelletto, N., Ferronato, M., Gambolati, G., Janna, C., Cairo, E., Marzorati, D.,  
791 Colombo, D., Ferretti, A., Bagliani, A., Bottazzi, F., 2011. Geomechanical response to  
792 seasonal gas storage in depleted reservoirs: A case study in the Po River basin, Italy. *J.*  
793 *Geophys. Res.* 116, F02002, doi:10.1029/2010JF001793.

794 Teatini, P., Tosi, L., Strozzi, T., Carbognin, L., Cecconi, G., Rosselli, R., Libardo, S., 2010.  
795 Resolving land subsidence within the Venice Lagoon by persistent scatterer SAR  
796 interferometry. *Physics and Chemistry of the Earth, Parts A/B/C*, In Press, Corrected  
797 Proof, doi:10.1016/j.pce.2010.01.002.

798 Vasco, D. W., Rucci, A., Ferretti, A., Novali, F., Bissell, R. C., Ringrose, P. S., Mathieson, A.  
799 S., Wright, I. W., 2010. Satellite-based measurements of surface deformation reveal  
800 fluid flow associated with the geological storage of carbon dioxide, *Geophys. Res.*  
801 *Lett.* 37, L03303, doi:10.1029/2009GL041544.

802 Vasco, D.W., Ferretti, A., Novali, F., 2008a. Estimating permeability from quasi-static  
803 deformation: temporal variations and arrival time inversion. *Geophysics* 73(6), O37–  
804 O52.

805 Vasco, D.W., Ferretti, A., Novali, F., 2008b. Reservoir monitoring and characterization using  
806 satellite geodetic data: interferometric synthetic aperture radar observations from the  
807 Krechba field, Algeria. *Geophysics* 73(6), WA113–WA122.

808 Zebker, H., Villasenor, J., 1992. Decorrelation in interferometric radar echoes; *Geoscience*  
809 *and Remote Sensing, IEEE Transactions on* 30(5), 950-959.

810 **Table caption**

811

812 Table 1: Aquifer homogeneous properties used for the spatio- temporal analysis of the surface  
813 vertical displacements

814

Aquifer property	Symbol	Value	Unit
Intrinsic permeability	$k$	$1.e^{-13}$	m <sup>2</sup>
Porosity	$\omega$	15	%
Thickness	$H$	50	m
Salinity	$sal$	150	g/l
Rock matrix compressibility	$c_{rock}$	$4.5e^{-10}$	Pa <sup>-1</sup>
Young's modulus	$E$	15	GPa
Poisson's ratio	$\nu$	0.25	-
Biot's coefficient	$b$	1.0	-

815

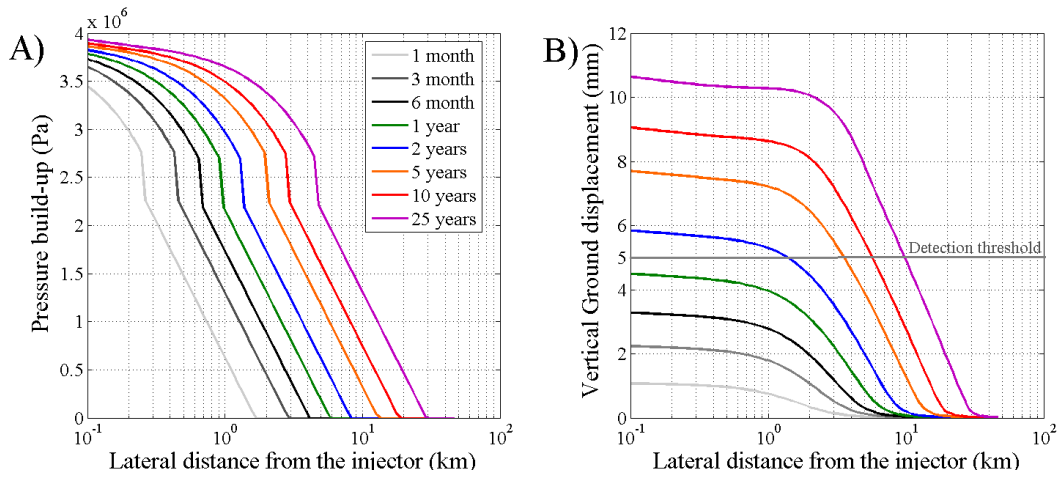
816

817 Table 2: Summary of the constraints on the implementation of the PSI technique and on the  
818 sensor regarding the specificities of the deformation phenomenon associated with CO<sub>2</sub>  
819 injection at depth

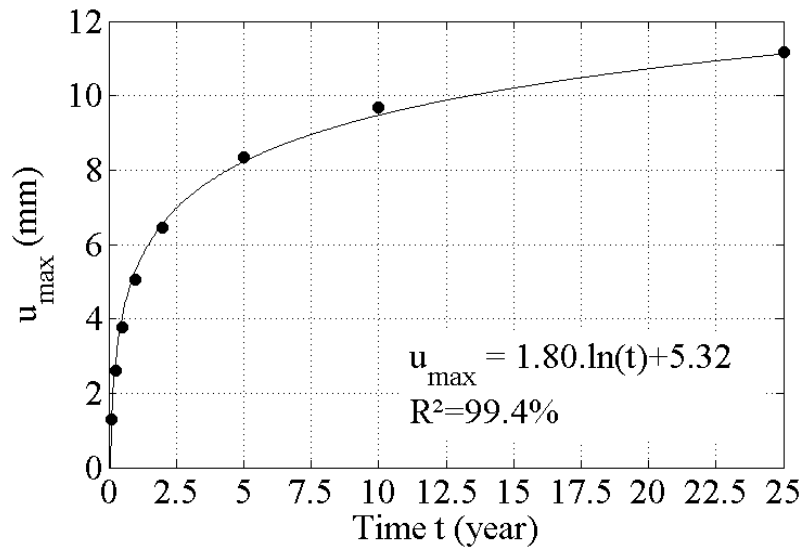
Expected deformation characteristics	Corresponding constraints on the implementation of the PSI technique and on the sensor
Large spatial scales tens of km)	- Large swaths (>50 km) are required;
Large vegetated areas	- Poor PS density is expected. Additional Corner Reflectors could be required to complement "natural" PS network.
Long term monitoring (25 – 50 years)	- Because of limited sensors lifetimes, the use of different successive satellites is required; - High sensor repetitiveness (typically, ten of days or better)

	<p>could reduce (respect to Envisat/ASAR-like configurations) the transition period between sensors by providing a minimum data archive to start the PSI processing (about 30 images) in the shortest possible duration;</p> <ul style="list-style-type: none"> <li>- Lifetime of PS are expected to be improved on small isolated areas with high density PS allowed by the use of high resolution image data;</li> <li>- Large amount of data are expected to be acquired, hence implying considering flexible and low-price data provision policies.</li> </ul>
<p>Spatio – temporal evolution of the deformation phenomenon</p>	<p>The acquisition and processing rate should be adapted to the expected spatio- temporal evolution of the deformation phenomenon. Based on simulations on a typical injection scenario:</p> <ul style="list-style-type: none"> <li>- the regions, where the deformation front passes, should be highly-rated sampled for a 2-4 years period;</li> <li>- the changes in the velocities values of the differential displacements are expected to be detectable only after a few months, implying a processing rate of 3 to 6 months.</li> </ul>
<p>Potentially sudden unexpected ground movements on localized areas</p>	<p>To fulfil the “early-warning” objective of the monitoring, a complement should be envisaged so that well definite zones at risk (such as fault zones) should be monitored using high repetitiveness / high resolution (but reduced swath) image data.</p>

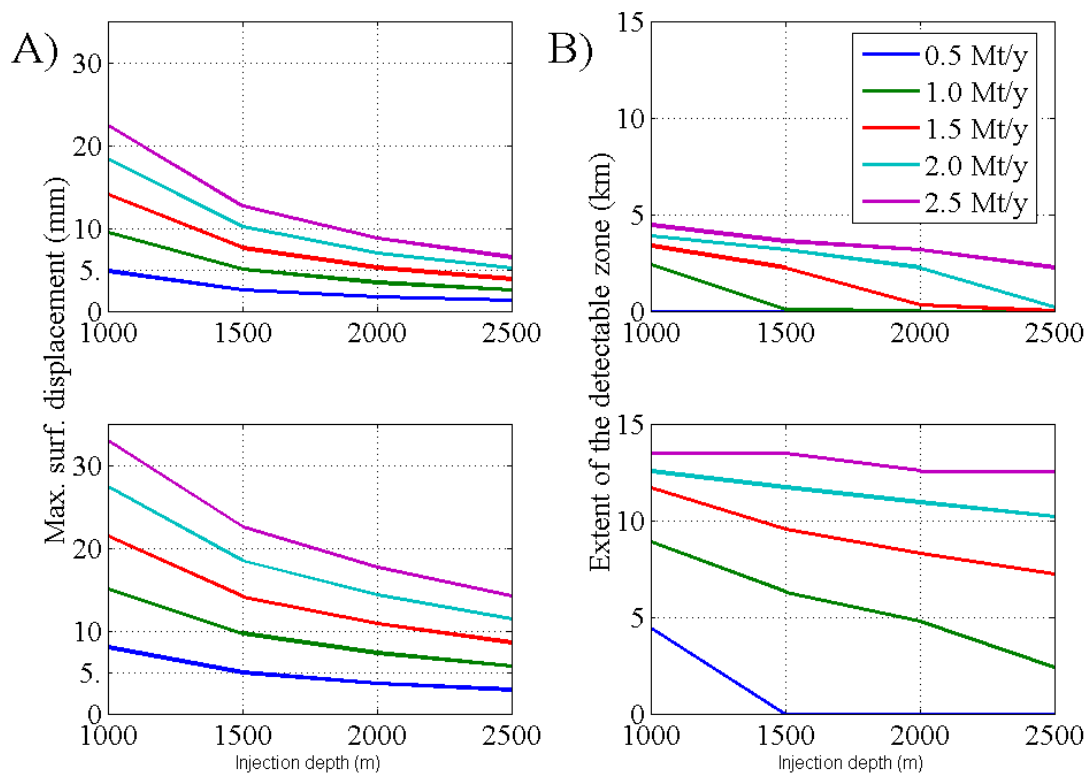
820 **Figure captions**



821  
 822 Figure 1: A) Pressure build-up (Pa) within the storage aquifer for a 1Mt/y CO<sub>2</sub> injection  
 823 scenario into a 1500m deep aquifer (considering the aquifer properties in Table 1); B) Vertical  
 824 displacement (mm) at the surface induced by the injection at depth. Detection threshold at 5  
 825 mm (discussed in section 2.1) is outlined by a grey-coloured horizontal line.



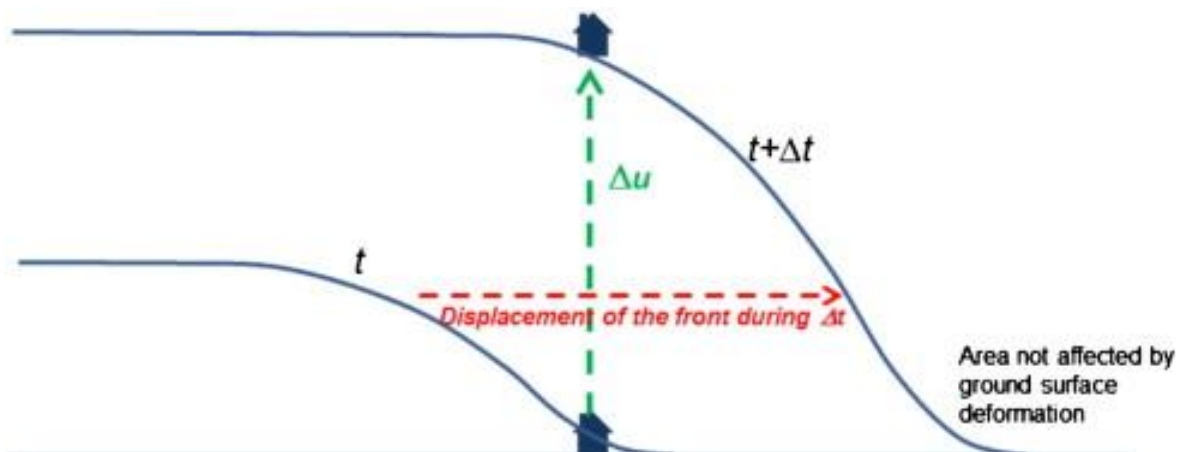
826  
 827 Figure 2: Temporal evolution of the maximum vertical displacement  $u_{\max}$  (mm) within the  
 828 injector zone for a 1Mt/y CO<sub>2</sub> injection scenario into a 1500m deep aquifer (considering the  
 829 aquifer properties in Table 1).



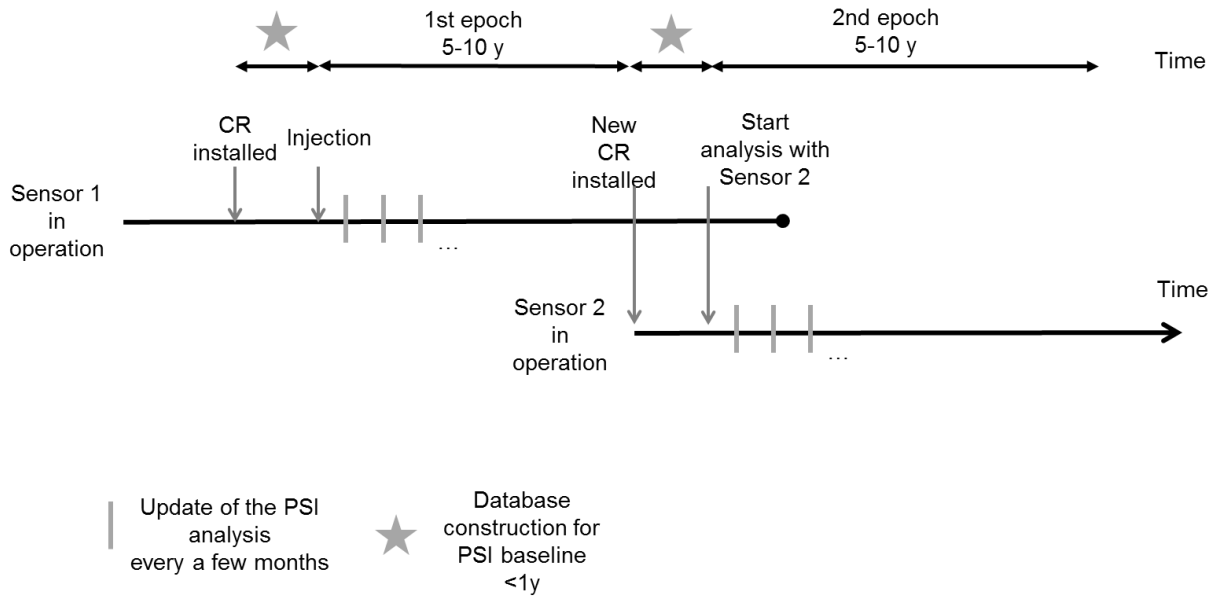
830

831 Figure 3: A) Maximum vertical displacement reached at the surface respectively after 1 and  
 832 10 years (top and bottom panels) considering different injection scenarios (mass injection  
 833 rates and depths) and the aquifer properties described in Table 1; B) Corresponding lateral  
 834 extent (km) of the detectable zone at the surface given a threshold of 5 mm respectively after  
 835 1 and 10 years (top and bottom panels).

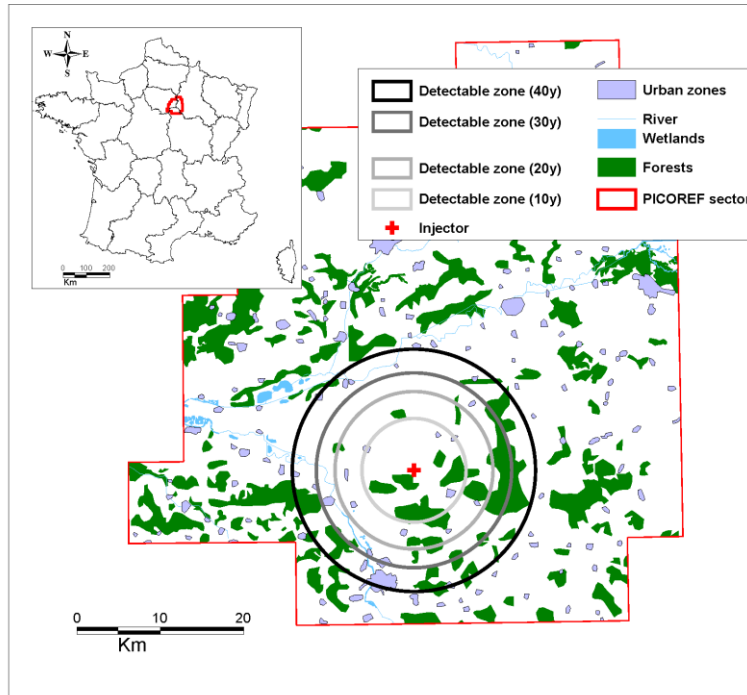
836



837 Figure 4: Schematic representation of the deformation to be measured.  $t$  corresponds to the  
 838 beginning of the front pass on the measurement point,  $\Delta t$  the duration of the front pass.  $\Delta u$  is  
 839 the resulting displacement on the observation point.

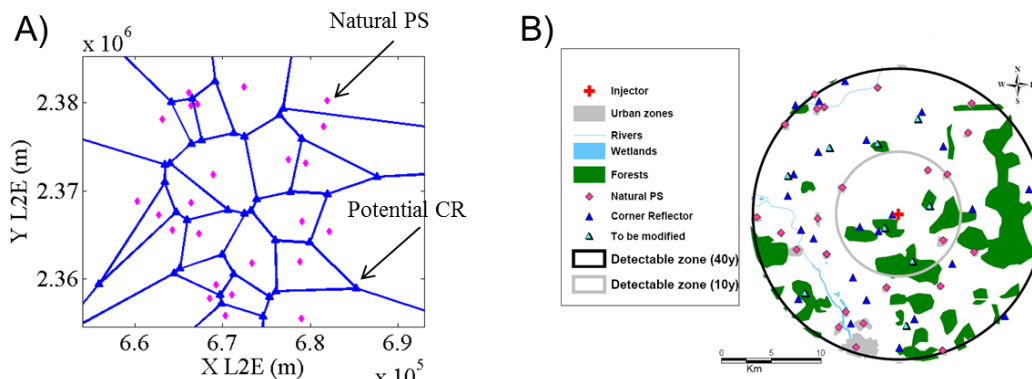


840  
 841 Figure 5: main steps for the application of the PSI analysis for “verification” monitoring using  
 842 CR and considering the transition period between successive satellite mission (sensor 1 and 2  
 843 with possible different characteristics). The duration of the PSI baseline step (outlined by a  
 844 star-like marker) is estimated considering a minimum of 30 images with a repetitiveness of a  
 845 ten of days. The processing rate every a few months is estimated based on the spatio-  
 846 temporal evolution of the deformation phenomenon associated with the typical injection  
 847 scenario described in section 1.2. This should be adjusted in case of the detection of a  
 848 “abnormal behaviour” (see discussion in section 2.4).



849

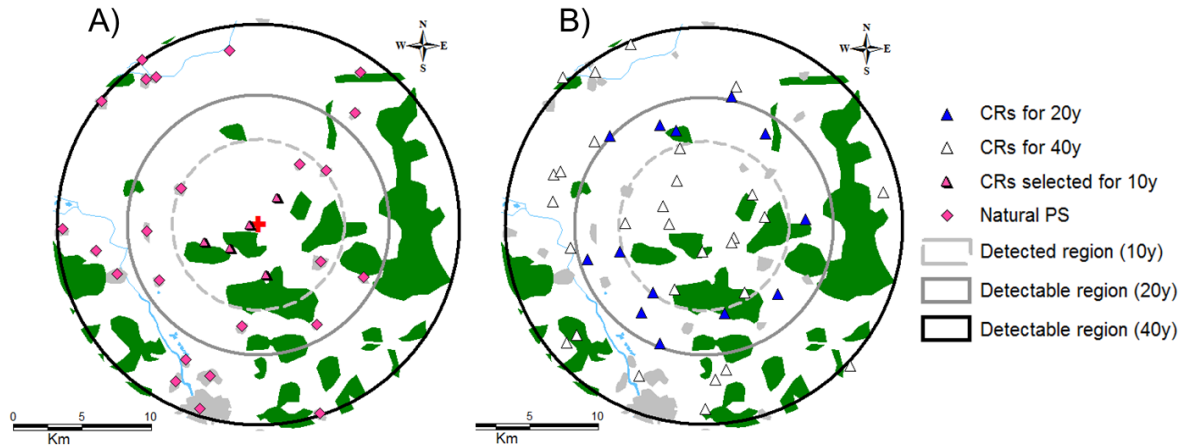
850 Figure 6: Location of the PICOREF sector (Grataloup et al. 2008) in the Paris basin context  
 851 (red line). The red cross marker represents the potential injector position selected based on the  
 852 risk analysis of Bouc et al. (2011). The circles represent the lateral extents of the expected  
 853 detectable zones (5mm threshold) for different time durations considering a 2Mt/y injection  
 854 scenario.



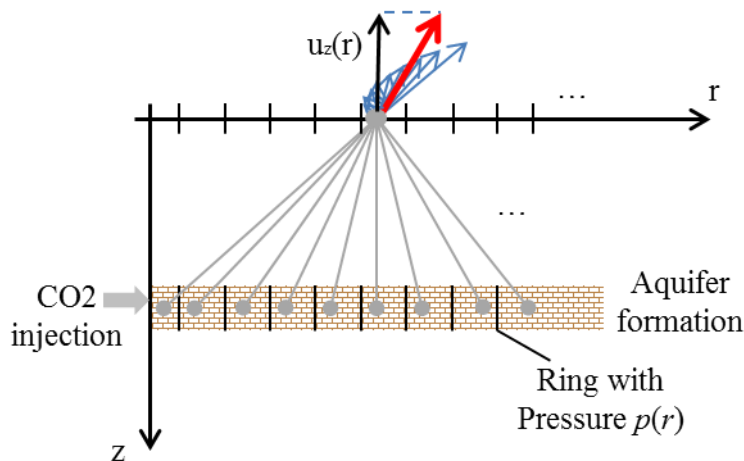
855

856 Figure 7: A) Voronoi analysis: pink coloured diamond markers represent natural PS located  
 857 within the detectable zone expected for the whole duration of the injection (black circle, see  
 858 right figure); blue coloured triangular markers represent potential CR at the edge of the  
 859 Voronoi cells depicted by blue segments. B) Application to the PICOREF sector for the first

860 10-years epoch. Light blue coloured triangular markers outline the CR lying within forest  
 861 zones or at a distance inferior to 1km to the neighbouring CR. Only the CR located within the  
 862 area bounded by the light grey-coloured circle are integrated for the monitoring of the  
 863 expected detectable zone for the first 10 years of injection.



864 Figure 8: A) network of natural PS (pink coloured diamond markers) completed with the CR  
 865 selected in the first 10-years epoch (pink coloured triangular markers); The dashed light grey  
 866 coloured circle represents the detected surface deformation after 10 years of injection; The  
 867 dark grey and black coloured circles respectively represent the expected detectable  
 868 deformation regions after 20 and 40 years of injection. B) identification of the CR (blue  
 869 coloured triangular markers) adapted for the monitoring of the next 10-years epoch (20 years)  
 870 based on the CR identified for the whole injection duration of 40y (white triangular markers).  
 871



872

873 Figure 9: Schematic representation of the cumulative contribution (light blue coloured arrows)  
874 of the rings of dilation with magnitude proportional to the reservoir pore pressure spatial  
875 distribution  $p(r)$  to the ground displacement (red arrow) at the lateral distance  $r$ . The vertical  
876 ground displacement  $u_z(r)$  is represented by a vertical black arrow.  
877